HiSST: International Conference on
High-Speed Vehicle Science Technology

26–29 November 2018, Moscow, Russia

Numerical study of wave trains in high-speed boundary layer over a cone

Andrey V. Novikov[1, 2]

Abstract

Direct numerical simulations of three-dimensional wave trains propagating in a boundary layer over 7° half-angle sharp cone at the freestream Mach number 5.95 are carried out. The Navier–Stokes equations are integrated using the in-house HSFlow solver implementing an implicit finite-volume shock-capturing method. Unsteady disturbances are imposed via a local suction-blowing actuator working at a fixed comparatively low frequency. The forced disturbances are transformed into a three-dimensional wave train dominated by oblique waves of the first mode. The disturbances grow downstream and ultimately exhibit weak nonlinear harmonics interactions in case of the moderate forcing level or demonstrate nonlinear breakdown into a "young" turbulent wedge in case of stronger forcing. Comparison is made with the controlled experiments at ITAM SB RAS, Novosibirsk performed on a cone with a disturbances actuator of glow discharge type. The computed azimuthal wavenumber spectra in case of moderate forcing are in good agreement with the experimental data. This and similar numerical simulations help to setup and interpret controlled experiments in wind tunnels as well as investigate laminar-turbulent transition mechanisms in boundary layer at high speeds.

Keywords: *DNS, high-speed boundary layer, aerodynamic instability, non-linear unstable mode interaction, cone*

Nomenclature

Latin

M – Mach number
Re – Reynolds number
p – non-dimensional pressure normalized by the doubled dynamic pressure
f – frequency

Greek

β – azimuthal component of the wave number
θ – azimuthal angle around the cone axis
ϕ – cone half-angle
ε – disturbances actuator forcing level
ω – angular frequency

Superscripts

$'$ – disturbance
$*$ – dimensional

Subscripts

0 – stagnation value
a – disturbances actuator
g – cone generatrix
w – wall
∞ – free stream

1. Introduction

Laminar-turbulent transition (LTT) in compressible boundary-layer flows is one of the major unsolved problems of high-speed aerodynamics. Since LTT leads to significant increases in heat transfer, reliable estimates of LTT locations are needed to predict the aero-thermal loads and surface temperatures. LTT also has a significant effect on the aerodynamic performance of a flying vehicle because of a substantial increase of the skin friction.

In the case of low free-stream disturbances typical for flight conditions, LTT includes the three main stages [1]: receptivity to external disturbances; growth of unstable modes (such as first and second

[1] *Central Aerohydrodynamic Institute (TsAGI), Zhukovsky, Russia, andrey.novikov@tsagi.ru*
[2] *Moscow Institute of Physics and Technology (State University) (MIPT), Dolgoprudny, Russia*

Mack modes, cross-flow instability and Görtler vortices); nonlinear breakdown of disturbances leading to a fully turbulent flow regime. Physical mechanisms relevant to these stages can be investigated experimentally or numerically.

For systematic investigations of linear and especially nonlinear stages of LTT, the "controlled" experiments are most suitable. However, due to technical difficulties in carrying out such experiments at high speeds, relatively few efforts of this type have been reported in the literature. First controlled experiments on a sharp cone in hypersonic flow have been performed by Maslov et al. [2] at ITAM SB RAS, Novosibirsk. These measurements were done on a 7° half-angle sharp cone model of 500 mm length in the T-326 hypersonic blowdown wind tunnel at $M_\infty = 5.95$. The disturbances were triggered by a glow discharge system generating frequencies related to the first (≈ 80 kHz) and second mode (≈ 280 kHz) of compressible boundary layer. Such a local-in-space actuator worked continuously, so that a harmonic in time 3D disturbance set in just downstream of the actuator. This disturbance is called hereafter a wave train. The spatially unstable wave train amplifies downstream and ultimately breakdown to a turbulent wedge. The obtained experimental data is rather limited, so it is worth to support it with direct numerical simulations (DNS).

In direct numerical simulation (DNS) approach the complete Navier–Stokes equations are solved by proper numerical methods without making restrictions on the basic (unperturbed) flow and disturbance amplitudes. DNS is well suited for a holistic modeling of the all LTT stages including nonlinear breakdown and provides a complete data of spatial and temporal disturbed flow evolution. In the present paper DNS are carried out by solving the 3-D Navier–Stokes equations for unsteady compressible flows of viscous perfect gas using the in-house solver "HSFlow" (High Speed Flow solver). Simulated is a wave train propagating in the boundary layer on a sharp cone at the freestream Mach number 5.95 and the Reynolds number ~ 13 millions per meter. The flow parameters are relevant to the experiments [2] and another DNS [3] performed using essentially different method. Main features of the instability development in the linear and nonlinear stages are explored using disturbance spectra, visualizations of 3D disturbance fields.

2. Problem formulation and numerical method

2.1. Governing equations

The equations to be solved are the 3D unsteady Navier–Stokes equations in conservative dimensionless form. The fluid is a perfect gas with the specific heat ratio $\gamma = 1.4$ and Prandtl number $\mathrm{Pr} = 0.72$. The dynamic viscosity is calculated using Sutherland's law $\mu = T^{3/2}(S+1)/(S+T)$, where $S = 110\,\mathrm{K}/T^*_\infty$. The Cartesian coordinates are normalized to a reference length L^*. The dependent variables are normalized to the corresponding freestream parameters, and pressure – to the doubled dynamic pressure $\rho^*_\infty U^{*2}_\infty$. Hereafter asterisks denote dimensional quantities. The details of the governing equations used for the DNS may be found in e.g. [4].

2.2. Numerical method

The Navier–Stokes equations are integrated using the in-house solver HSFlow (High Speed Flow), which implements an implicit finite-volume shock-capturing method with the second-order approximation in space and time. Godunov-type TVD scheme with Roe approximate Riemann solver is used. Reconstruction of dependent variables at the grid cell boundaries is performed using WENO (Weighted Essentially Non-Oscillatory) approach, which effectively gives the third-order space approximation. The system of nonlinear algebraic equations, which approximates the governing partial differential equations, is solved using the Newton iteration method. At every iteration step, the corresponding linear algebraic system is solved using the GMRes (Generalized Minimal Residual) method. Note that this approach is universal and most efficient if the computational domain contains shock waves and other strong spatial inhomogeneities of the flow such as boundary-layer separations. Despite dissipative nature of the shock-capturing method, the HSFlow solver allows numerical simulations of boundary-layer stability including configurations with separation bubbles [5, 6, 7].

Table 1. Free-stream flow parameters

M_∞	5.95	T^*_∞	$48.635\,\mathsf{K}$
$\mathsf{Re}_{\infty,1}$	$12.78\times10^6\,\mathsf{m}^{-1}$	T^*_0	$393\,\mathsf{K}$
γ	1.4	T^*_w	$338\,\mathsf{K}$
Pr	0.72	ϕ	7°
		L^*	$0.1\,\mathsf{m}$

The HSFlow solver employs MPI technology and PETSc framework for distributed calculations on high-performance computing clusters. For parallel computations, the source structured grid is split into multiple zones with one-to-one interzone connectivity. The resulting algebraic equations are solved collectively by parallel methods implemented in PETSc library. The details on numerical method may be found in [4].

2.3. Flow parameters

Considered is a hypersonic flow at free-stream Mach number $\mathsf{M}_\infty = 5.95$ over a sharp $\phi = 7^\circ$ half-angle cone at zero angle of attack. The flow parameters correspond to the stability experiments [2] in controlled conditions in T-326 wind tunnel at ITAM SB RAS, Novosibirsk and are recapitulated in Table 1. The reference values for de-dimensionalizing are $L^* = 0.1\,\mathsf{m}$ and free-stream velocity magnitude $V^*_\infty = \mathsf{M}_\infty\sqrt{\gamma R T^*_\infty} = 831.62\,\mathsf{m}\cdot\mathsf{s}^{-1}$. With that $\mathsf{Re}_\infty \equiv \mathsf{Re}_{\infty,L} = 1.278\times10^6$.

Three-dimensional computational domain is shown in Fig. 1. It was created by rotating the 2-D domain about x-axis in the range of transversal angle $0 \le \theta \le 90^\circ$, with that $y = x\,\mathsf{tan}(\phi)\,\mathsf{cos}(\theta)$, $z = x\,\mathsf{tan}(\phi)\,\mathsf{sin}(\theta)$. The cone nose tip bluntness was correctly resolved with radius $r^* = 0.1\,\mathsf{mm}$ (nominally sharp). The length of the computational domain $l^*_x \approx 310\,\mathsf{mm}$ (shorter than experimental model size $500\,\mathsf{mm}$).

The boundary conditions are: no-slip conditions on the wall; the free-stream conditions on the outer boundaries; the linear extrapolation from the interior for the dependent variables on the outflow boundary and $y = 0$ plane; the symmetry condition at $z = 0$ plane.

2.3.1. Disturbances actuator

The problem is solved in two steps. First, a steady laminar flow field (base flow) is computed using the time-dependent method. Then, unsteady disturbances are imposed onto the base flow via the actuator modeled using the boundary condition for vertical mass-flow perturbation

$$(\rho v)_w = \varepsilon\left(1-r^6\right)\left(\frac{1}{2}\,\mathsf{sin}\left(\omega_a t\right) + \frac{1}{2}\,\mathsf{sin}\left(2\omega_a t\right)\right),$$
$$r(x,z) = \frac{2}{d}\sqrt{\left(x-x_0\right)^2+z^2},\; x_0 - \frac{d}{2} \le x \le x_0 + \frac{d}{2},\; -\frac{d}{2} \le z \le \frac{d}{2}$$

Here $x_a = 0.69$ ($x^*_a = 69\,\mathsf{mm}$) and $d = 0.005$ ($d^* = 0.5\,\mathsf{mm}$) are central point and diameter of the actuator according to the experiment. This unsteady boundary condition imitates suction and blowing through a short circular channel, where the flow does not yet resemble the Poiseuille quadratic profile but have more abrupt profile $\sim r^6$.

Computations are done for the actuator working continuously at fixed frequency $\omega_a = 59$ (frequency factor $\omega_a/\mathsf{Re}_\infty = 4.617\times10^{-5}$) corresponding to the experimental value $f^*_a = 78\,\mathsf{kHz}$ which addresses the first-mode instability. The periodic glow discharge consists of recurring short pulses containing higher-harmonics in frequencies, so a second harmonic at doubled frequency $2\omega_a$ is added in the present simulation.

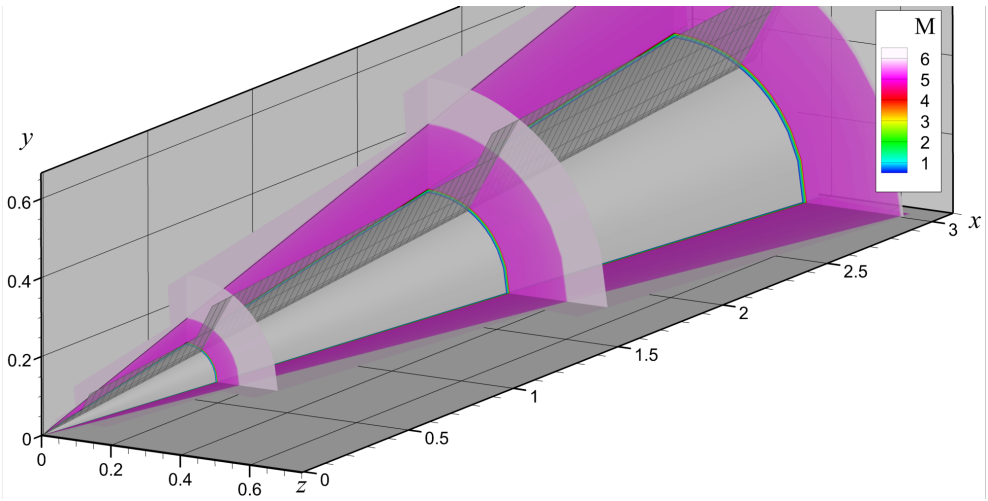

Fig 1. Computational domain and Mach numbers fields of steady flow in several cross-sections. Semi-transparent gray plane denotes the beginning of buffer zone

The amplitude of the initial disturbance achieved in the experiment is unknown. In the present DNS three variants of forcing levels are considered: the low

$$\varepsilon = 0.0025,$$

the moderate

$$\varepsilon = 0.03$$

and the high

$$\varepsilon = 0.05.$$

2.4. Numerical simulation parameters

The orthogonal structured multiblock grid with $5001 \times n_y \times 101$ nodes (137 millions in total) was used for computations. The grid step along the cone generatrix is $\Delta x_g = 6.2 \times 10^{-4}$, in the normal direction inside the boundary layer $\Delta y_g = 1.13 \times 10^{-4}$ (~120 grid lines), in azimuthal direction $\Delta\theta = 0.35°$. In the range $30.7° < \theta \leq 90°$ there is a buffer (sponge) zone where the grid cell size gradually enlarges upto huge values max $\Delta\theta \approx 16°$ to increase numerical dissipation and dump outgoing disturbances.

The time step during disturbances simulations is $\Delta t = 0.0005$, i.e. one period of initial fluctuations $2\pi/\omega_a = 0.1$ is represented by 213 steps.

For disturbances simulations, the sharp nose region at $x \lesssim 0.59$ was cut out from the grid resulting in lower dimension of 117.5 million nodes.

Computations were carried out using multiprocessor high-performance computing cluster with distributed memory. Upto 886 CPU cores were employed simultaneously for a single case.

3. Results

The computed steady laminar flow over the cone is shown in Fig. 1. Because of the viscous–inviscid interaction, a weak shock wave is formed near the cone nose. It is seen that the shock do not cross the domain top boundary. The boundary layer near the wall is also clearly seen.

The periodic forcing imposed onto the steady boundary layer generates a 3-D wave train evolving downstream. Its instantaneous footprint on the wall is shown in Fig. 2 using wall pressure disturbance fields $p'_w(x, z)$. Hereafter the disturbance (or pulsation) fields $q'(t)$ are obtained by subtracting the basic flow

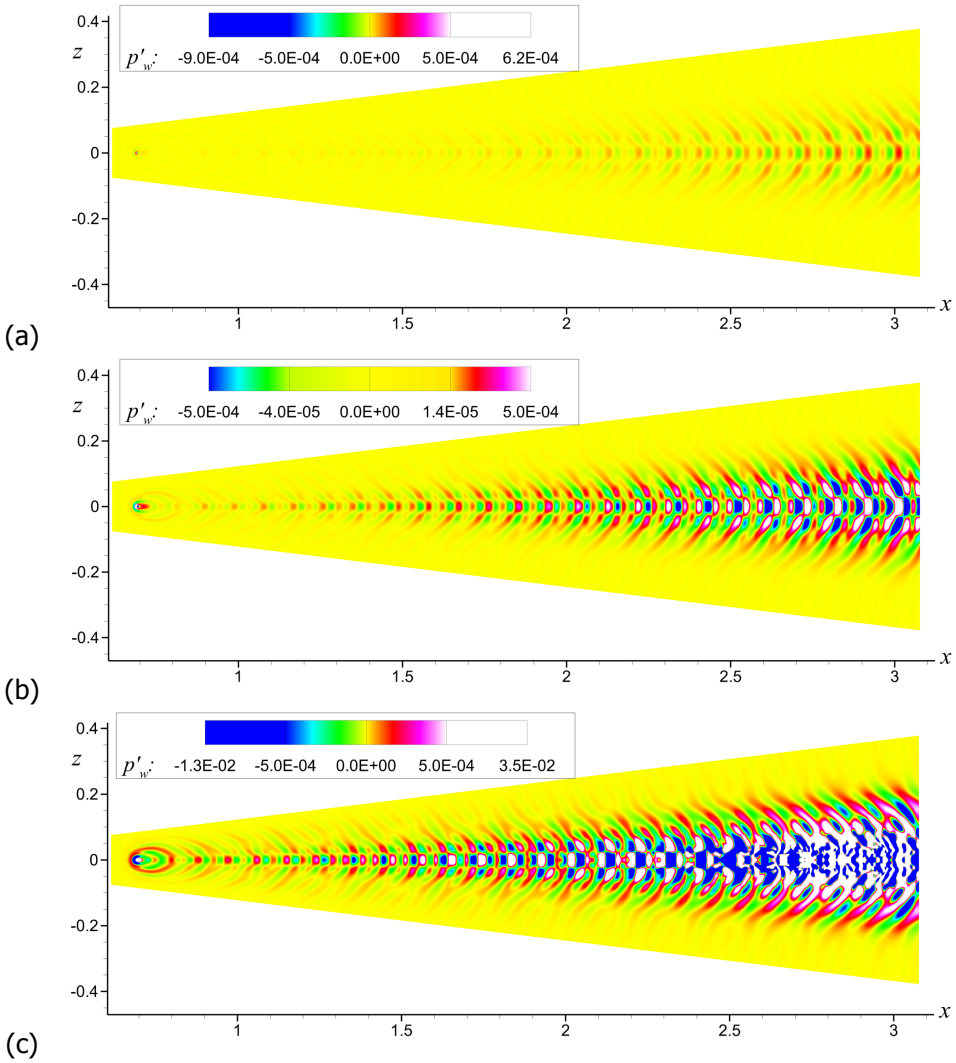

Fig 2. Instantaneous wall pressure disturbance fields for different forcing levels: a) $\varepsilon = 0.0025$, b) $\varepsilon = 0.03$, c) $\varepsilon = 0.05$

field from the total field at a particular time instant, $q'(t) = q(t) - q(t = 0)$. For convenience the patterns shown hereafter are obtained by mirroring of the computed flow field versus the $z = 0$ symmetry plane.

Initially, the wave fronts emanating from the forced area are elliptic. As the disturbance propagates, the waves became oblique and V-shaped pattern is formed. This is typical for the first-mode dominated disturbance. Visible wave fronts are not uniform due to the superposition of waves with different front angles.

The disturbance amplitude grows monotonically downstream as it is seen in Fig. 2. In case of the high forcing level $\varepsilon = 0.05$, the amplitude ultimately reaches a critical level and nonlinear breakdown to turbulence begins. This is manifested as small-scale random-like structures in the disturbances pattern (Fig. 2c).

Figure 3 shows 3-D vortical structures in the disturbed boundary layer. The vortices are identified by Q–criterion, where Q is the second invariant of the velocity gradient tensor $Q = \frac{1}{2}\left[|\Omega|^2 - |S|^2\right]$ with

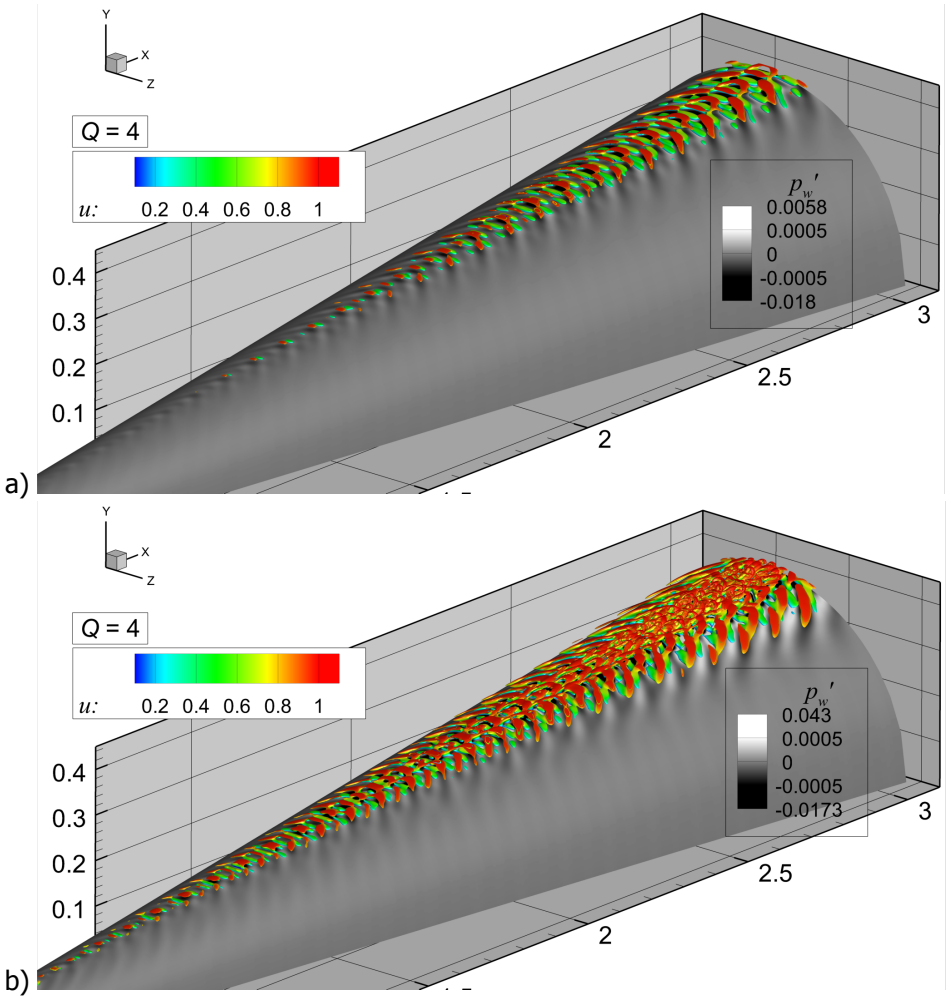

Fig 3. Vortices in the disturbed boundary layer as the isosurfaces of Q-criterion $Q = 4$ colored with u-velocity magnitude. Also shown is wall pressure disturbance field. The forcing is at $\varepsilon = 0.03$ (a) and $\varepsilon = 0.05$ (b).

$S = \frac{1}{2}\left[\nabla V + (\nabla V)^T\right]$ and $\Omega = \frac{1}{2}\left[\nabla V - (\nabla V)^T\right]$. In case of the moderate forcing (Fig. 3a), the vortices exhibit large-scale regular-in-space structures corresponding to the oblique waves of carrier frequencies ω_a and $2\omega_a$. With the high level of forcing, random-like small-scale vortices fill up the central portion of the wave train surrounded by oblique waves. This is typical for the turbulent wedge.

The side view of this "young" turbulent wedge in the symmetry plane $z = 0$ is shown in Fig. 4 using the shadowgraph pattern ($\nabla^2\rho$). Outside the disturbed boundary layer the acoustic waves are clearly seen, that resembles the noise produced by a turbulent boundary layer.

In experiments [2] the mass-flow pulsations $(\rho u)'$ were measured at some distance from the cone surface where these pulsations reach the maximum amplitude. The same data was extracted from the time sequence of the computed 3-D fields. The procedure resulted in 2-D oscillograms $(\rho u)'(x_{fix}, h_{fix}, \theta; t)$ for the several x-sections $x = x_{fix}$, where h_{fix} is the maximum pulsations layer.

The two dimensional Fourier spectra of the mass-flow pulsations in the cross-section $x = 2.24$ are shown in Fig. 5 for different actuator amplitudes. In case of the low forcing level $\varepsilon = 0.0025$, the disturbances evolve linearly and the spectrum exhibits two oblique waves of ω_a and $2\omega_a$ frequencies with similar azimuthal wavenumbers $\beta_\theta \approx \pm 0.3$ (Fig. 5a). For moderate forcing level $\varepsilon = 0.03$, the spectrum at

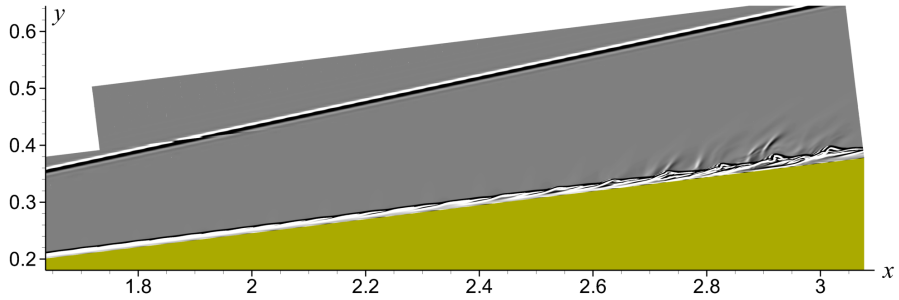

Fig 4. Instantaneous shadowgraph of the disturbed boundary layer in the symmetry plane $z = 0$ in case of high forcing level $\varepsilon = 0.05$

frequency ω_a in addition to the main peaks $\beta_\theta \approx \pm 0.3$ exhibit side peaks $\beta_\theta \approx \pm 0.7$. Apparently, these side peaks are the effect of weak nonlinear subharmonic interactions between waves of ω_a and $2\omega_a$ frequencies. This phenomenon is described in detail in [3], where experiment [2] was also numerically simulated. The spectrum in the case of high forcing $\varepsilon = 0.05$ is much broader and illustrates the strong nonlinear process of boundary layer breakdown into turbulence.

The normalized azimuthal wavenumber β_θ spectra of computed mass-flow pulsations at the base frequency ω_a in two x cross-sections are shown in Fig. 6 for low and moderate forcing levels. Also plotted are the spectra obtained in the experiment [2] with unknown initial disturbances amplitude. Numerical and experimental spectra are in very good agreement. The curves are qualitatively the same, the amplitude growth from the first to the second x-position is quantitatively the same and the main peaks $\beta_\theta \approx \pm 0.3$ agrees perfectly. More over, for the moderate forcing level the additional side peaks $\beta_\theta \approx \pm 0.7$ related to the subtle nonlinear sub-harmonic interactions effect are reproduced in DNS.

In the case of high actuator amplitude, the computed azimuthal wavenumber β_θ spectrum shown in Fig. 7 is essentially different in comparison to the experimental one. This indicates that the glow discharge actuator in the experimental study [2] generated disturbances of rather low amplitude and did not trigger the strong nonlinear processes.

4. Summary

Three-dimensional wave trains propagating over a 7° half-angle sharp cone at zero angle of attack at the freestream Mach number 5.95 were studied numerically. Simulated were the experiments on stability performed at ITAM SB RAS on a cone using artificial disturbances induced by a periodic electric glow discharge actuator. In DNS, unsteady disturbances were imposed using local forcing of the vertical mass-flow on the wall. This point-source actuator produces wave trains that evolve downstream and excite first-mode mode instabilities. Three different forcing levels were considered. The modeling were performed by numerical solution of Navier–Stokes equations using the in-house HSFlow solver that implements an implicit finite-volume shock-capturing method of second-order approximation is space and time.

The computed disturbances spectra were compared with the experimental data and a very good agreement was shown in the case of appropriate forcing level. In particular, the simulated azimuthal wavenumber distributions capture the subtle effect of nonlinear interactions between fundamental and subharmonic waves. It is shown that specifying the correct forcing level in DNS is essential to precisely model the experiment. Too weak forcing leads to fully linear disturbances evolution without nonlinear interactions. Too strong forcing leads to nonlinear breakdown to turbulence.

This and similar numerical simulations may help to setup, perform and interpret experiments in controlled conditions in hypersonic wind tunnels as well as develop holistic models of laminar-turbulent transition at high speeds.

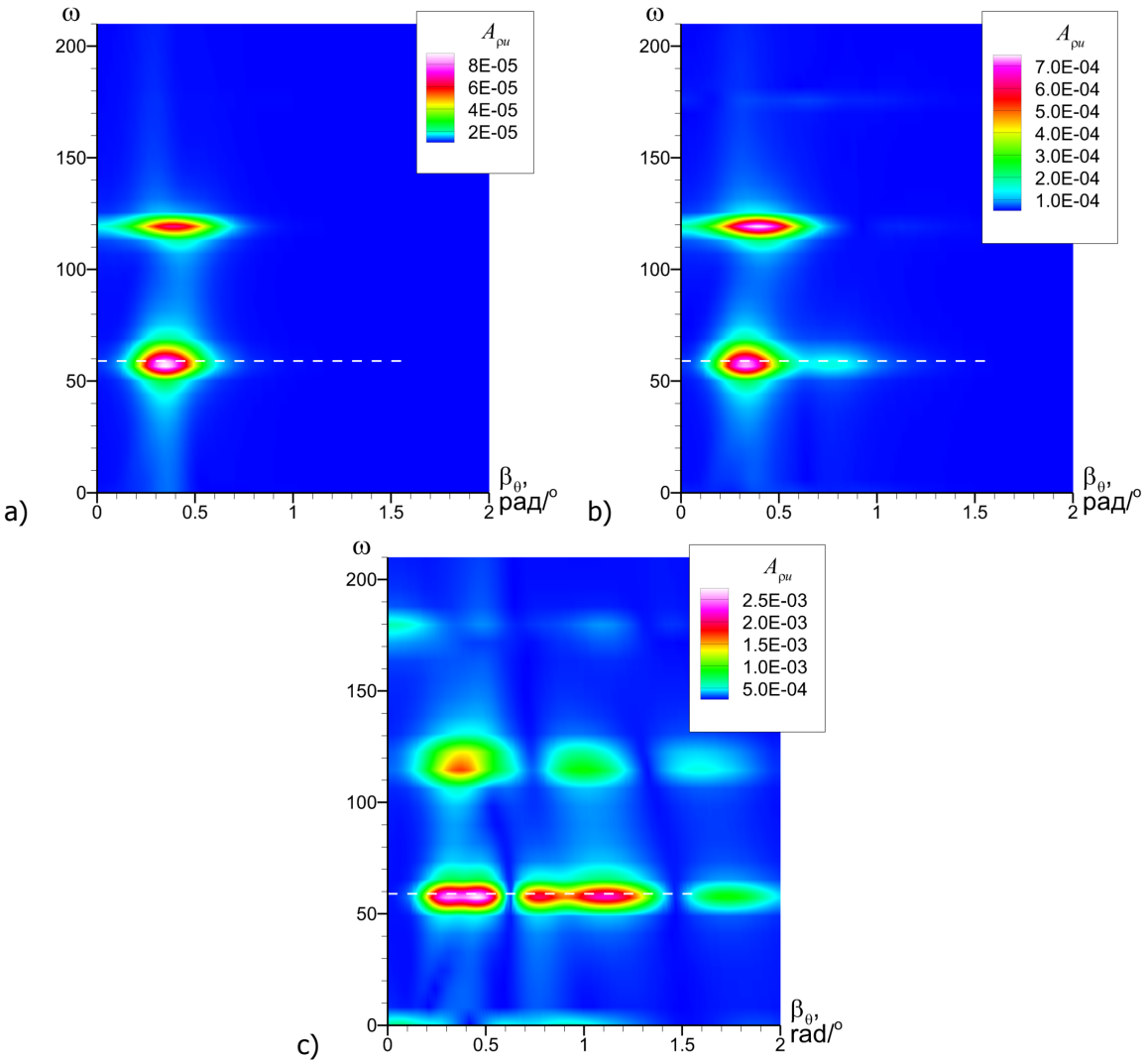

Fig 5. Spectra of mass-flow pulsations $(\rho u)'$ in the maximum pulsations layer at cross-section $x = 2.24$ for forcing levels $\varepsilon = 0.0025$ (a), $\varepsilon = 0.03$ (b) and $\varepsilon = 0.05$ (c). The dashed line denotes the carrier frequency ω_a.

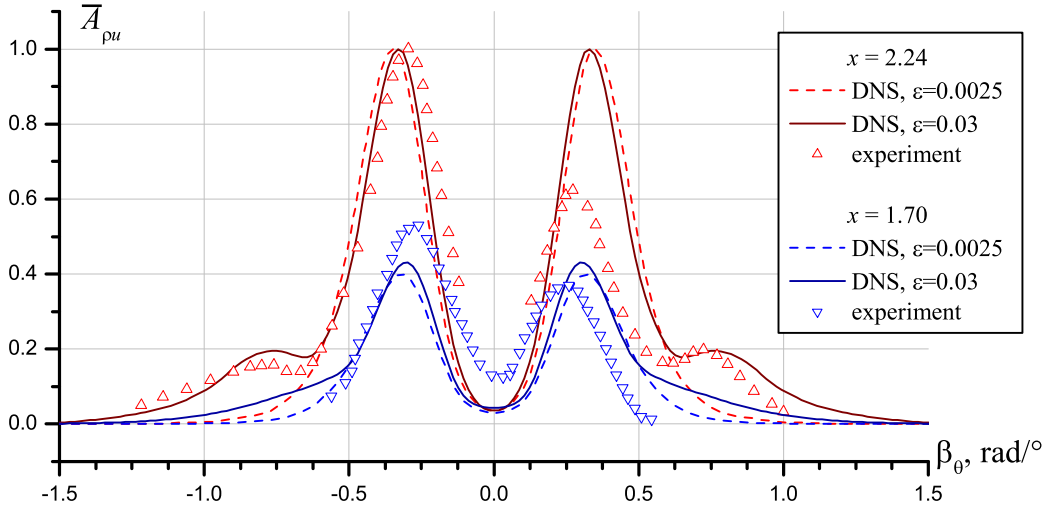

Fig 6. Normalized azimuthal wavenumber spectra of $(\rho u)'$ at $\omega_a = 59$ and different x-sections for low and moderate forcing levels. DNS – present work; experiment – [2]

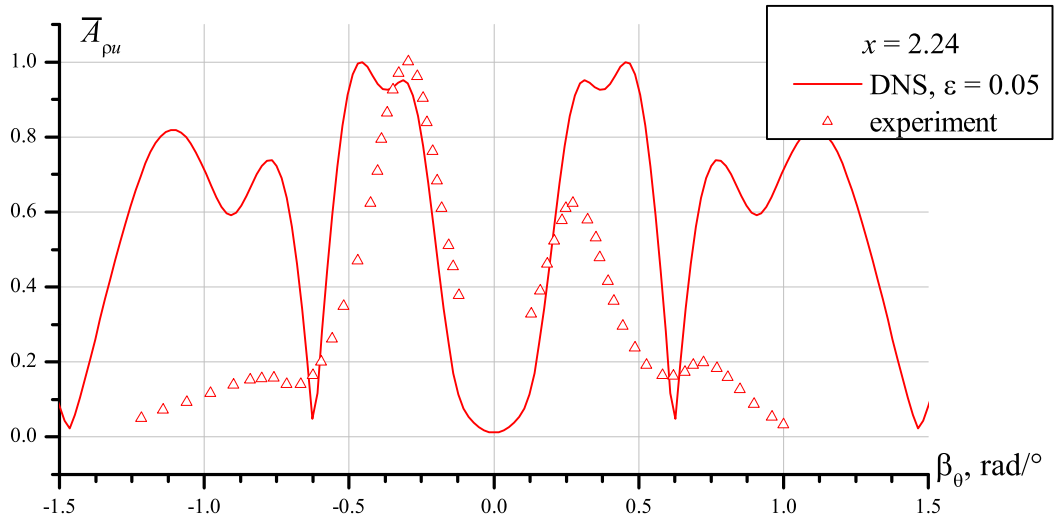

Fig 7. Normalized azimuthal wavenumber spectrum of $(\rho u)'$ at $\omega_a = 59$ for high forcing level. DNS – present work; experiment – [2]

This work has been carried out at Moscow Institute of Physics and Technology (MIPT) using computing resources of the federal collective usage center Complex for Simulation and Data Processing for Mega-science Facilities at NRC "Kurchatov Institute", http://ckp.nrcki.ru/ with financial support of the Russian Scientific Foundation (project No. 14-19-00821 – computations, postprocessing) and the Russian Foundation for Basic Research (project No. 18-08-01295 – development of the disturbances actuator model; project No. 16-08-01200 – development of software tools for fields postprocessing).

References

[1] Fedorov, A.: Transition and Stability of High-Speed Boundary Layers. Annual Review of Fluid Mechanics, 43(1), 79–95 (2011). https://doi.org/10.1146/annurev-fluid-122109-160750

[2] Maslov, A., Shiplyuk, A., Sidorenko, A.: Study of hypersonic boundary-layer instability on a cone using artificial disturbances. In: Proc. International Conference on the Methods of Aerophysical Research (ICMAR), pp. 132 – 137 (2000).

[3] Fezer, A., Kloker, M.: Direct Numerical Simulation of Transition Mechanisms at Mach 6.8 on the flat plate and the cone. In: Aerodynamics and Thermochemistry of High Speed Flows (EuroMech Colloquium 440 (EMC-440)), 2002

[4] Egorov, I., Novikov, A., Fedorov, A.: Direct numerical simulation of the laminar--turbulent transition at hypersonic flow speeds on a supercomputer. Computational Mathematics and Mathematical Physics, 57(8), 1335--1359 (2017). https://doi.org/10.1134/S0965542517080061

[5] Bountin, D., Chimitov, T., Maslov, A., Novikov, A., Egorov, I., Fedorov, A., Utyuzhnikov, S.: Stabilization of a Hypersonic Boundary Layer Using a Wavy Surface. AIAA Journal, 51(5), 1203--1210 (2013). https://doi.org/10.2514/1.j052044

[6] Novikov, A., Egorov, I., Fedorov, A.: Direct Numerical Simulation of Wave Packets in Hypersonic Compression-Corner Flow. AIAA Journa, 54(7), 2034--2050 (2016). https://doi.org/10.2514/1.J054665

[7] Novikov, A.: Transition Induced by a Wave Train in a Supersonic Boundary Layer over a Compression Ramp. In: 47th AIAA Fluid Dynamics Conference (2017). https://doi.org/10.2514/6.2017-4517